Investigation of SnO_2-modified $LiMn_2O_4$ Composite as Cathode Material for Lithium-ion Batteries

Li Wang, Jishi Zhao, Shaohua Guo, Xiangming He[*]*, Changyin Jiang, Chunrong Wan*

Institute of Nuclear & New Energy Technology, Tsinghua University, Beijing 100084, PR China
[*]E-mail: hexm@tsinghua.edu.cn

SnO_2-modified $LiMn_2O_4$ cathode materials are prepared based on controlled crystallization and solid state reaction. SEM analysis shows that SnO_2-modified samples have the same spherical shape as unmodified ones. Powder X-ray diffraction (XRD) analysis reflects that obtained peaks correspond well with characteristic of spinel structural $LiMnO_4$ samples in the range of 5° and 90°. Based on XRD and ICP-AES analysis it may safely be concluded that some SnO_2 particles have been introduced (doped) into the crystal matrix of $LiMn_2O_4$, while other SnO_2 particles agglomerate on the surface of $LiMn_2O_4$ which is evidenced by EDXS analysis. EDXS analysis reveals that some SnO_2 particles are coated on the surface of the $LiMn_2O_4$ during the preparation processes. Furthermore, the influence of the SnO_2 on the electrochemical performance of $LiMn_2O_4$ is characterized by electrochemical impedance spectroscopy (EIS) and cyclic voltammetry (CV). In comparison to unmodified samples, SnO_2-modified samples exhibited better cycling performance from 76.3 mAh g^{-1} to 99.6 mAh g^{-1} and higher capacity retention from 67.8% to 95.1% at 55^oC after 50 cycles.

1. INTRODUCTION

Although widely used in the field of various portable electric devices as a power supply, lithium ion batteries have still attracted much attention in attempts to ameliorate the performance of their inside components. Owing to such advantages as low cost, low toxicity and high safety, spinel $LiMn_2O_4$ can be used as cathode material of lithium ion batteries in place of $LiCoO_2$. Many researches on Li-Mn-O compounds have been reported in recent years [1-7]. However, $LiMn_2O_4$ suffers from a drastic capacity fading after long-term cycling, which has a great detrimental impact on its practical

application. It is postulated that this problem is induced by the dissolution of $LiMn_2O_4$ electrode into electrolyte (as Mn^{2+}) and a phase transition due to Jahn-Teller distortion [8].

Doping and coating have been widely applied to improve the electrochemical performance of $LiMn_2O_4$. Above all, doping can alleviate Jahn-Teller effect, resulting in stabilized spinel structure of $LiMn_2O_4$.Furthermore; doping can decrease the dissolution of Mn^{2+} (according to equation (1)) due to the fact that dopant ions might take the place of Mn^{3+} in $LiMn_2O_4$. Such metals as Al, Mg, Zn and Ni [3-5, 9-10] have been adopted as dopants to enhance the performance of the spinel $LiMn_2O_4$. Some researchers have found that the coated spinel $LiMn_2O_4$ shows not only a good rate capability, but also an improved tolerance to overcharging and elevating temperature performance due to the increased conductivity [11-13].

$$2Mn^{3+}_{solid} \rightarrow Mn^{4+}_{solid} + Mn^{2+}_{solution} \qquad (1)$$
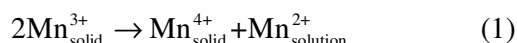
However, He et al. [14] found that doping of yttrium could enhance the activity of manganese in spinel $LiMn_2O_4$, which cause the active manganese to dissolve into electrolyte easily during cycling. In this work, SnO_2-modified $LiMn_2O_4$ samples were prepared by solid phase synthesis at high temperature. During the preparation processes, the doping of SnO_2 maybe occurred in the surface layer of pristine $LiMn_2O_4$, and some SnO_2 powders are coated on the surface of $LiMn_2O_4$ simultaneously. Mn^{4+} ions were partially replaced by Sn^{4+} after doping in an attempt to increase the concentration of Mn^{3+} on the surface, and at the same time, induce more Mn^{2+} dissolution into electrolyte. In present work, X-ray diffraction (XRD), scanning electron microscopy (SEM), energy dispersive X-ray spectroscopy (EDXS), electrochemical impedance spectroscopy (EIS) and cyclic voltammetry (CV) were applied to investigate the physical characteristics and electrochemical properties of the SnO_2-modified $LiMn_2O_4$ samples.

2. EXPERIMENTAL

2.1. Preparation and characterization of Sn-doped LiMn₂O₄ powders

Firstly, spherical $MnCO_3$ powders were synthesized by controlled crystallization method [15-16] via a chemical reaction as follows:

$$MnSO_4 + 2NH_4HCO_3 \rightarrow MnCO_3 \downarrow + (NH_4)_2SO_4 + H_2CO_3 \quad (2)$$
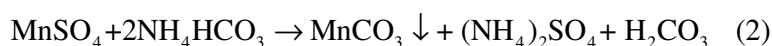
Here, $MnSO_4$, NH_4HCO_3, and $NH_3\bullet H_2O$ solutions were fed continuously into a crystallization reactor with agitation. All particles formed in the reactor gradually with a spherical shape after a definite reaction time. The spherical Mn_2O_3 was then obtained by heat-treatment of $MnCO_3$ at 560°C for 4h. A mixture of Mn_2O_3, Li_2CO_3 and SnO_2 was calcined at 750°C for 20h to produce the composites. The weight percentages of SnO_2 in as-prepared composites were 0, 1%, 2%, 5% and 10%,

respectively. In this paper, we describe these samples as pristine LMO, Sn (1%)/LMO, Sn (2%)/LMO, Sn (5%)/LMO and Sn (10%)/LMO, respectively.

The crystal structure of the samples was characterized by X-ray diffraction (XRD, Rigaku, D/max-rB) using a diffractometer with Cu Kα radiation. Morphologies and energy dispersion X-ray spectroscopy (EDXS, point scanning mode) of the synthesized samples were observed with scanning electron microscopy (SEM, JSM-6301, Hitachi, Ltd.). After every sample immerged in the electrolyte at room temperature for 72h, the dissolved manganese was detected by inductively coupled plasma-atomic emission spectrum (ICP-AES, Thermo-Jarrell-Ash IRIS).

2.2. Electrochemistry measurements

The as-prepared composite was mixed with acetylene black and PTFE in weight ratio of 8:1:1 to form slurry. After solvent evaporation, the electrode was prepared and dried at $120^{\circ}C$ under vacuum over 24h. CR2025-type coin cells were assembled in a glove box (M. Braun GmbH, Germany) with H_2O and O_2 content below 2ppm. Metallic lithium foil was used as counter electrode. The electrolyte was 1M $LiPF_6$ dissolved in EC + DEC (1:1, v/v) and Celgard 2400 polyethylene membrane was used as separator.

Electrochemical impedance spectroscopy (EIS) and cyclic voltammetry (CV) analysis were carried out using ZAHNER-IM6eX electrochemical workstation. EIS measurements were performed with 10 mV perturbation amplitude in the range from 100 kHz to 5 mHz in automatic sweep mode from high to low frequency. The impedance spectra were recorded at each state allowing at least 5 additional hours for equilibration after each charge step. The counter electrode was lithium foil about 1.0 cm^2 and the electrochemical measurements were performed with a two-electrode system. Data acquisition and analysis were made using the electrochemical impedance software. CV was carried out within a voltage range of 2.5V ~ 4.5V at the scan rate of 0.2mV s^{-1}. All the electrochemical measurements mentioned above were conducted at room temperature. The research on cycling performance was conducted between 4.35 V and 3.35 V with a current density of 0.5mA/cm^2 at room temperature and $55^{\circ}C$.

3. RESULTS AND DISCUSSION

3.1. Physical characteristics

3.1.1. XRD results

Fig.1 shows the XRD patterns of the composite powders with different content of SnO_2 addition. The diffraction peaks marked as (111), (311), (400), (511) and (440) in the spectra correspond well with the standard data of JCPDS 35-0782 card, indicating the existence of the well-crystallized spinel cubic $LiMn_2O_4$ phase in all samples. Table 1 show that the lattice constants decrease with the increase of the amount of SnO_2, and the sample (e) has the smallest lattice constant. These

changes in the lattice constants reveals that some Sn^{4+} ions have been introduced into the crystal lattice of pristine $LiMn_2O_4$ in place of Mn^{4+} ions. Obviously, not all SnO_2 entered into the crystal lattice because changes in the lattice constants (decreasing from 8.248 to 8.2236 Å) are not comparable with SnO_2 content (increasing from 0 to 10%).
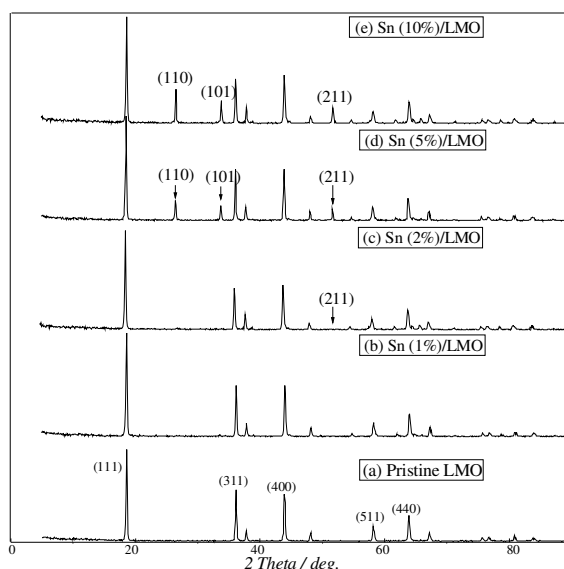

Figure 1. XRD patterns of (a): Pristine LMO, (b): Sn (1%)/LMO, (c): Sn (2%)/LMO, (d): Sn (5%)/LMO and (e): Sn (10%)/LMO

Furthermore, the diffraction peaks corresponding to SnO_2 marked as (110), (101) and (211) have been clearly observed in the patterns of sample (d) and (e) as well as a weak diffraction peak of SnO_2 (211) in the pattern of sample (c), indicating the existence of pristine SnO_2 particles in the composite.

Table 1. The lattice constants of different samples

Sample	Pristine LMO	(b)	(c)	(d)	(e)
Lattice constant/Å	8.248	8.2392	8.2374	8.2288	8.2236

3.1.2. SEM results

Fig. 2 shows SEM photos of the samples. It is definitely showed that all the samples are spherical with diameters less than 40 μm in Fig. 2. EDXS analysis shows the atomic percentage of the Sn element on the surface of the samples (b), (c), (d), and (e), as shown in Table 2. From Table 2, it can be observed that the content of Sn element on the surface is larger than the expected percentage, which is ascribed to the fact that most of SnO_2 particles have been coated on the surface of $LiMn_2O_4$.
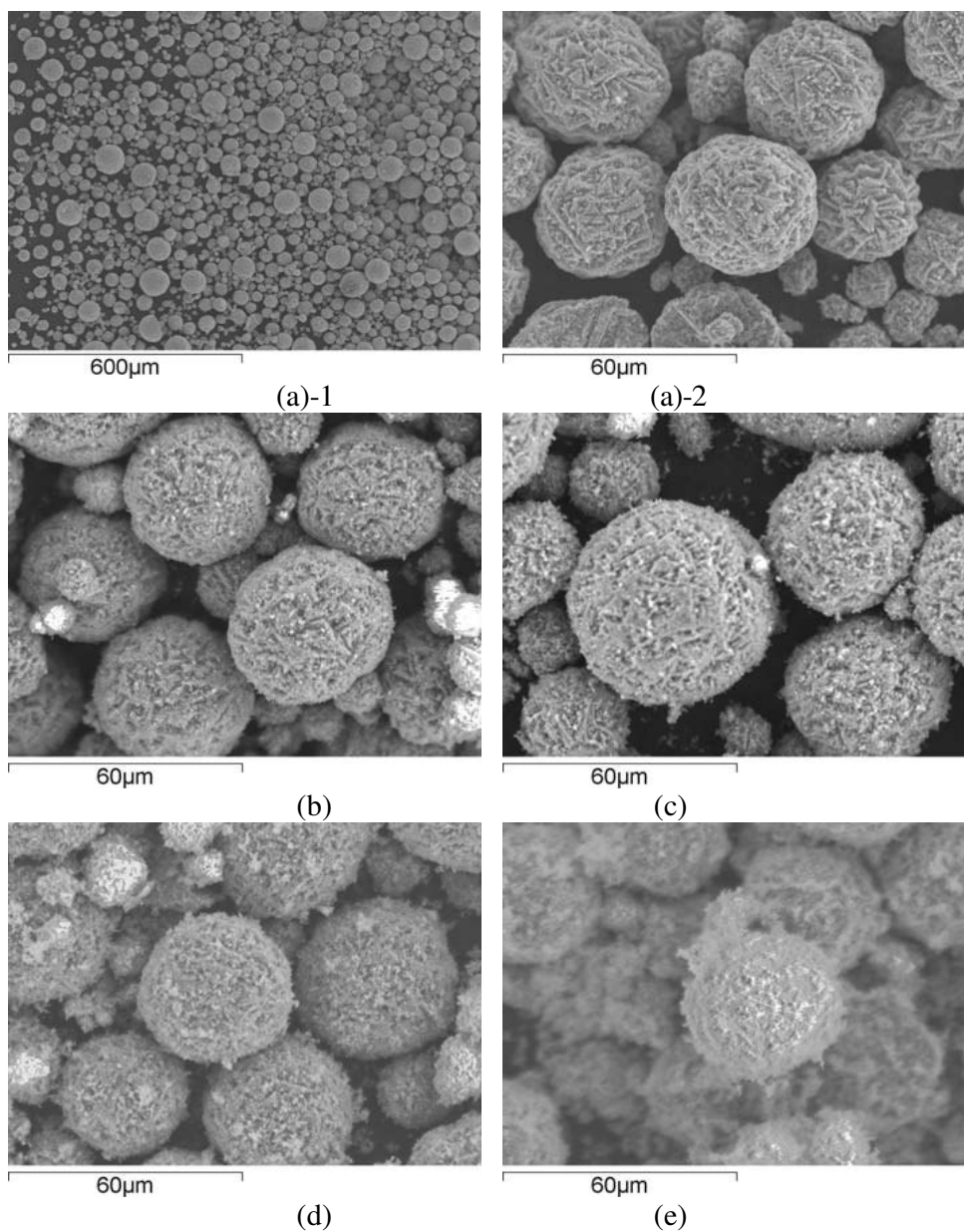
Figure 2. SEM of (a)-1 and (a)-2: Pristine LiMn$_2$O$_4$; (b): Sn (1%)/LMO, (c): Sn (2%)/LMO, (d): Sn (5%)/LMO and (e): Sn (10%)/LMO[41]

3.1.3. ICP-AES results

The ICP-AES results are presented in Table 3. As can be seen, the dissolution percentage of Mn of pristine LMO is the smallest, revealing that the addition of SnO$_2$ enhances the dissolution of Mn.

Table 2. Sn content on the surface of the spherical composites

samples	Sn (1%)/LMO	Sn (2%)/LMO	Sn (5%)/LMO	Sn (10%)/LMO
Sn percentage (wt. %)	1.98	4.04	8.5	17.71
Prospective percentage (wt. %)	1	2	5	10
Relative ratio	1.98	2.02	1.7	1.771

It is well known that Mn^{2+} is relatively easy to dissolve into the electrolyte. It can be inferred that some Mn^{4+} ions have been partially replaced by Sn^{4+} and consequently increased the ratio of Mn^{3+}/Mn^{4+} by addition of SnO_2. According to the ionic dissolution equilibrium, as shown in equation (1), more Mn^{2+} ions can readily be dissolved into electrolyte after the dissolution of Mn^{3+} ions. Moreover, the dissolution percentage of Mn decreased with the increase of SnO_2 content (from 1% to 10%), revealing that the doping of Sn^{4+} does not increase with the increase of SnO_2 content in the modified samples.

Table 3. the dissolution percentage of Mn

samples	Pristine LMO	Sn (1%)/LMO	Sn (2%)/LMO	Sn (5%)/LMO	Sn (10%)/LMO
Dissolution percentage/‰	0.65	2.45	1.97	1.14	0.97

3.2. Electrochemical results

3.2.1. Cyclic voltammograms

Fig. 3 shows the CV plots of the first and the tenth cycle (scan rate: $0.2mV\ s^{-1}$) obtained at room temperature. Both XRD and ICP-AES results have shown that some superfluous SnO_2 is coated on the surface of $LiMn_2O_4$, or exists in the composite as unexpected impurities during the preparation processes. As a result of the unexpected impurities, both C and E are different from the others, especially the 1st CV. There are no obvious differences in the tenth CV (dash dot line) from A to E, demonstrating that the influence of the surface layer doping and the impurities disappears after several cycles, and the SnO_2 coating on the surface prevents the Mn dissolution into electrolyte furthermore after several cycles. The integrated curves are used to calculate the quasi-thermodynamic *x* versus *E* curves in order to assign a value of the intercalation degree (*x*) to each potential. Nobili et al. [17] considered that the calculated *x* values probably contain some errors and should be taken with some care because of the small capacity loss (~1–2%) during the initial polarization process. From Fig. 3, it can be found that bigger capacity deterioration occurs in sample C and E, which maybe result from the relative higher content of SnO_2 on the surface of the $LiMn_2O_4$.
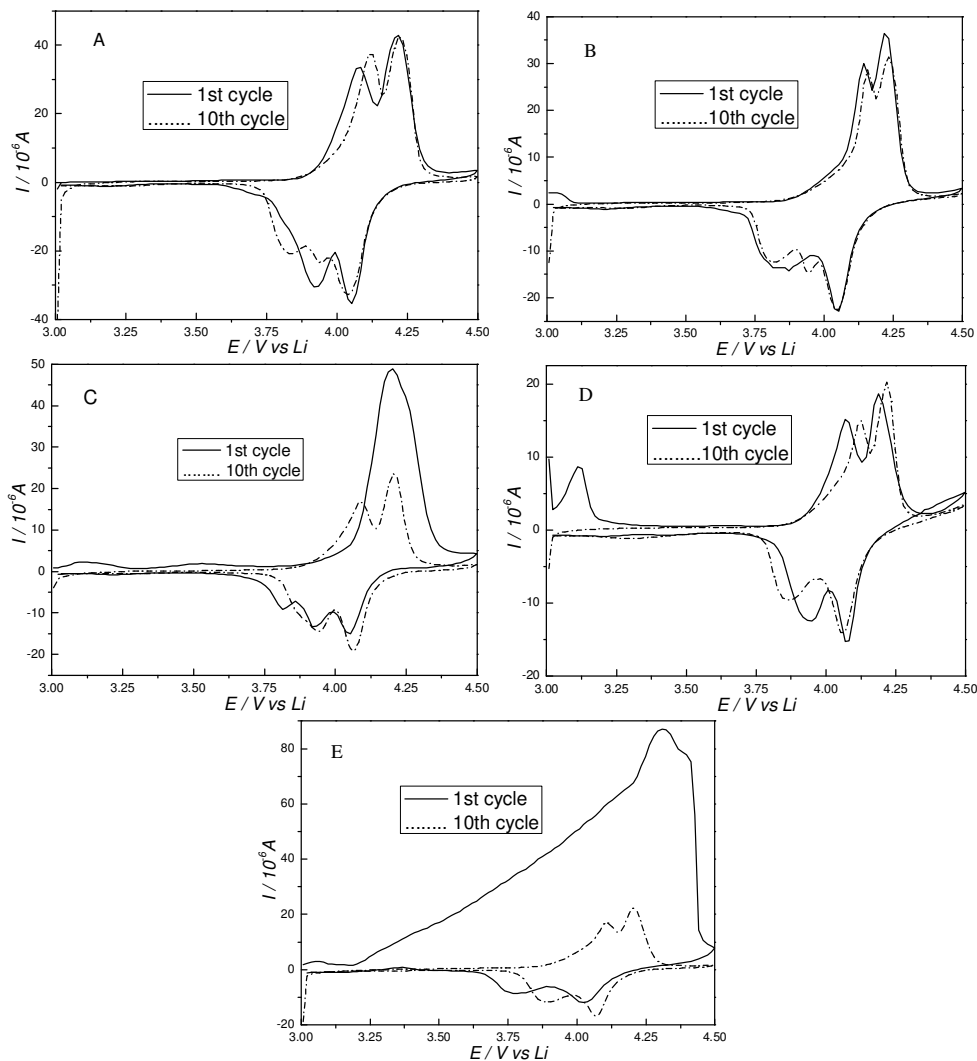
Figure 3. Cyclic votammograms of electrodes at 25°C (A: Pristine LMO, B: Sn (1%)/LMO, C: Sn (2%)/LMO, D: Sn (5%)/LMO and E: Sn (10%)/LMO, Scan rate: 0.2mV s^{-1})[41]

Moreover, the cation doping shows favorable influences on the electrochemical performance [18]: (1) the valence of Mn will be increased by doping, it is helpful to suppress Jahn-Teller effect; (2)the spinel frame of LiMn$_2$O$_4$ will be stabilized, it is helpful for lowering structural change during charge/discharge process and inhibiting the solution reaction of Mn; (3) the improvement of the conductivity is propitious to the reversible lithium intercalation and deintercalation and (4) the surface area will be decreased, resulting in the decrease of contacting area between active cathode materials and electrolyte.

The CV curves of all samples at the 10th cycle are quite similar, revealing the electrochemical stability of modified LiMn$_2$O$_4$. Anyway, the addition of SnO$_2$ exhibits significant influence on the cycling performance, as shown in the following sections.

3.2.2. Electrochemical impedance spectra

EIS is one of the most powerful tools to analyze electrochemical reactions, such as those processes occurring at electrode/electrolyte interfaces and the lithium ion intercalation/deintercalation occurring in anode/cathode, and has been widely reported in the previous literature [17, 19-26]. The Nyquist plots of electrochemical lithium ion deintercalation from oxide-based electrodes (corresponding to the charge processes) commonly consist of three parts: the first arc in the high frequency range, the second arc in the medium frequency range and an approximate straight line inclined at a constant angle to the real axis in the lower frequency range. Though the dependence of Nyquist plots for impedance spectra on state of charge (SOC) does not come to an agreement among researchers, it is acknowledged that every part of the plots can indicate some electrochemical characterizations of electrode materials [27-31, 42]. In this study, EIS is employed to investigate the influence of SnO_2 on the electrochemical performance of $LiMn_2O_4$, especially the resistance of solid electrolyte interface (SEI) film (R_{sf}), charge transfer resistance (R_{ct}) and the resistance between SEI film and cathode (R_{in}).
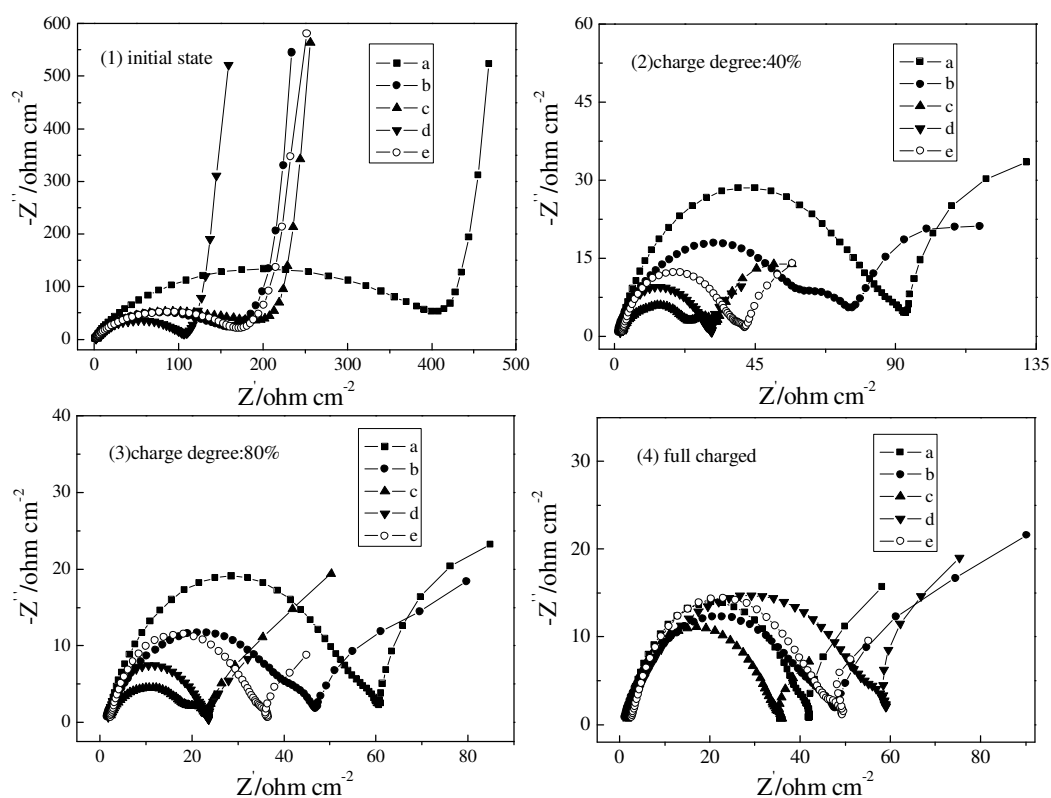

Figure 4. Series of Nyquist plots obtained at different state of charge at the rate of 0.1C (a: Pristine LMO, b: Sn (1%)/LMO, c: Sn (2%)/LMO, d: Sn (5%)/LMO and e: Sn (10%)/LMO)

Fig. 4 reveals a series of characteristic Nyquist plots obtained at different SOC. Each plot consists of a depressed semicircle or two semicircles in high and medium frequency regions. Thomas

et al. considered that the depressed arc belong to insertion compound [32]. It is shown that the EIS analysis of a pressed porous powder insertion compound electrode in contact with liquid electrolyte can be modeled by a modified Randles equivalent circuit using a resistor/capacitor (R/C) combination. In fact, the presence of an additional dipole may account for at least two physical processes [33-36]: one is an adsorption process of Li^+ ions or other species onto the surface of the electrode without charge transfer; the other is the formation of a surface layer on the electrode. According to not well defined semicircle (see inset in Fig. 4) presented at the high frequency limit, it can be speculated that the latter case occurring in this work, so the surface of electrode is probably covered by an ionically conductive but electrically insulating surface layer. The lithium ion diffusion region at the lower frequencies is generally assigned to solid state diffusion of lithium ion into the bulk cathode material [30].
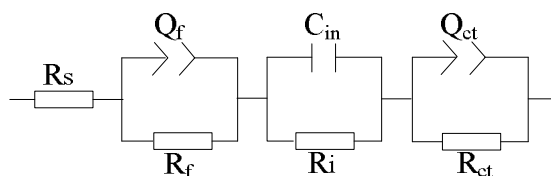

Figure 5. Equivalent circuit describing the impedance responses shown in Fig. 4

Generally, the overall impedance decreases with the decrease of the charge degree, and the semicircles in the high and middle frequency range are more defined at middle charged state, such as at 40% SOC. There are two distinct semicircles in the plots from (2) to (4), which is different from the plots (1). And the size of all the semicircles is strongly depended on the SOC. In order to investigate the Nyquist plots in detail, it is necessary to build an equivalent circuit to fit into the impedance spectra shown in Fig. 4. Such equivalent circuit has been shown in Fig. 5. In the equivalent circuit, R_s represents the ohmic resistance of the electrolyte; R_{sf} and R_{in} are resistances of SEI film and the interface between SEI film and cathode, respectively; R_{ct} is the resistance of the lithium ion transference in cathode. C_{in} represents the capacitance of the double layer; the capacitance of the SEI film and lithium ion diffusion impedance are represented by constant phase elements (CPE) Q_f and Q_{ct}, respectively. The expression for the CPE (Q) is

$$Y = Y_0 \omega^n \cos\left(\frac{n\pi}{2}\right) + jY_0 \omega^n \sin\left(\frac{n\pi}{2}\right) \qquad (3)$$

Where, ω is the angular frequency, j is the imaginary unit. A CPE represents a resistor when $n=0$, a capacitor with capacitance of C when $n=1$ and an inductor when $n=-1$. By the way, CPE represents a Warburg resistance when $n=0.5$ if Warburg resistance exists in impedance spectra.

The results were shown in Fig. 6. It is clearly showed that the changes in the charge degree (SOC) have no obvious influence on R_{sf} and R_{in} with respect to the sample of Sn (2%)/LMO by Fig.

6(1) and Fig. 6(2). Moreover, both resistances of the sample are smaller than those of other remaining samples. During the charge process the stability of R_{sf} and R_{in} is probably attributed to the surface coating of SnO_2. Fig. 6(3) shows that R_{ct} decreases with the increase of charge degree (from 0% to 100% SOC). R_{ct} is supposed to represent the lithium ion diffusion in the cathode. The value of R_{ct} is expected to decrease during the charge process because the ionic conductivity of cathode materials will increase with the deintercalation of lithium ion from host. Obviously, the addition of SnO_2 has a beneficial (positive) effect on the ionic conductivity of $LiMn_2O_4$ due to the fact that t R_{ct} is evidently decreased after the modification, as shown in Fig. 6(3). Furthermore, it is well noted that the sample of Sn (2%)/LMO shows the smallest R_{ct} among all the samples. Li et al. [37] have studied the influence of Sn doping on the diffusion coefficient of Lithium ion in electrode materials. It can be considered that the doping of Sn can not only stabilize the crystal structure, but also enhance the ionic conductivity of electrode materials. In this study, it has been demonstrated that the addition of SnO_2 reduces the impedance of R_{sf}, R_{in} and R_{ct} during the first cycle, which is conductive, favorable for the improvement of the cycling performance of $LiMn_2O_4$ cathode.

3.2.3. Cycling performance test

Table 4. Cycling performance of Li/composites cathode conducted between 4.35 V and 3.35 V with a current density of $0.5mA/cm^2$ at room temperature and 55^oC ($mAh\ g^{-1}$)

samples	Room temperature			55^oC	
	*	**	***	*	**
Pristine LMO	119.5	104.4/87.4%	93.7/78.4%	112.6	76.3/67.8%
Sn (1%)/LMO	117.6	99.4/84.5%	92.0/78.2%	104.1	94.7/91.2%
Sn (2%)/LMO	117.6	106.9/90.9%	100.7/85.6%	104.7	99.6/95.1%
Sn (5%)/LMO	106.7	102.4/96.0%	99.4/93.2%	93.1	86.0/92.4%
Sn (10%)/LMO	95.8	94.3/98.4%	90.6/94.6%	87.7	79.6/90.8%

Note: *---Initial capacity;

**---50th cycle capacity/capacity retention;

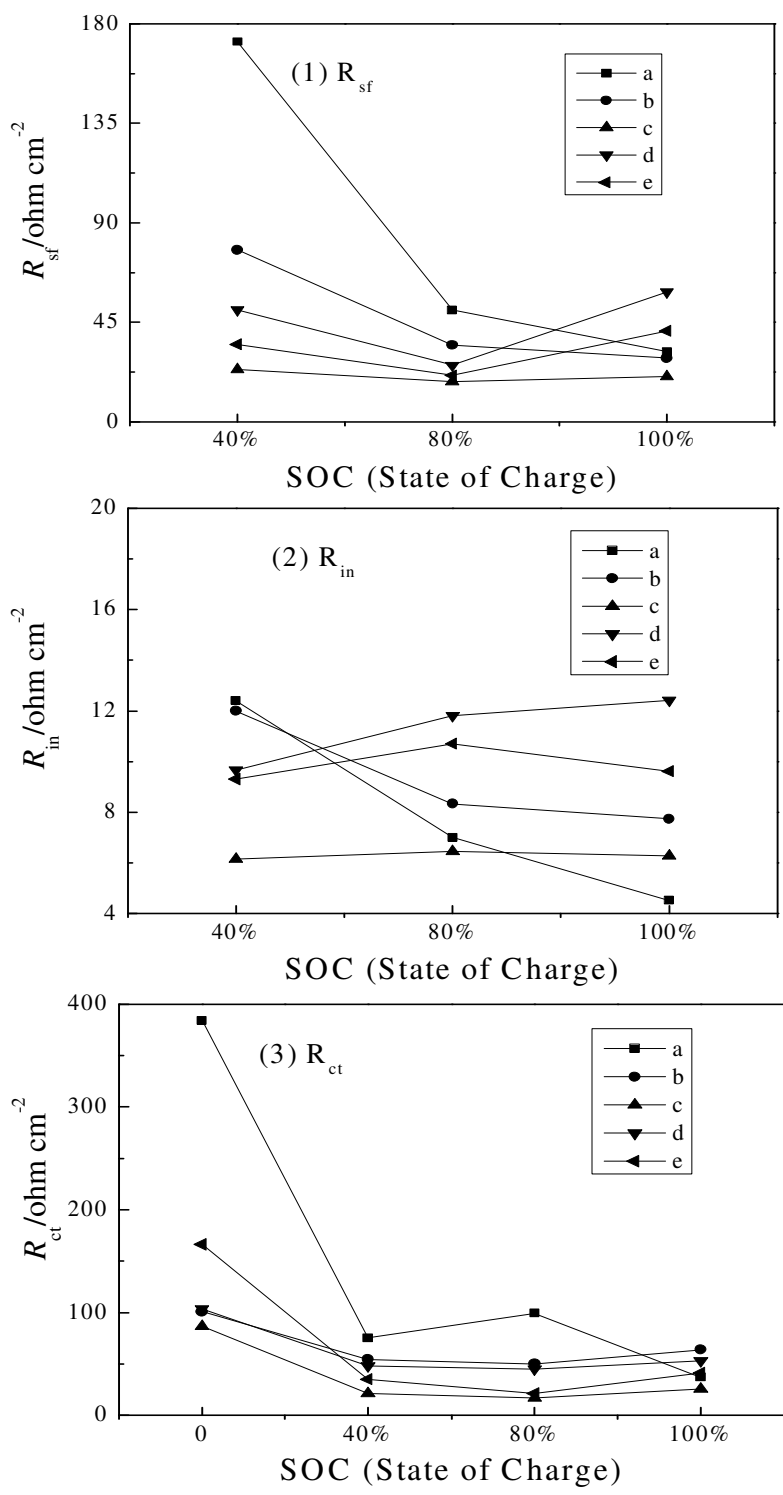***---100th cycle capacity/capacity retention.

Figure 6. Results of the Nyquist plots shown in Fig. 4 (a: Pristine LMO, b: Sn (1%)/LMO, c: Sn (2%)/LMO, d: Sn (5%)/LMO and e: Sn (10%)/LMO)

Table 4 shows the cycling performance of Lithium metal-pristine LMO (or SnO_2-modified samples) cell cycled between 4.35 V and 3.35 V with a current density of 0.5mA/cm^2 at room

temperature and 55°C. The initial capacity decreased with increase of the content of SnO$_2$ (wt. %) from 0 to 10% at room temperature and 55°C resulting from the surface layer doping of Sn^{4+}. The capacity retention at room temperature shows the same tendency, reflecting that the addition of SnO$_2$ improves the cycleability because of the moderate SnO$_2$ coatings on the surface of LiMn$_2$O$_4$. The capacity fading at higher temperatures (>50°C) is too high for practical applications [38-40] because the dissolution of LiMn$_2$O$_4$ electrode into the electrolyte (as Mn^{2+}) increases with the increase of temperature. In this work, the Sn (2%)/LMO composite displays the best cycling performance at 55°C, the capacity and the capacity retention increase from 76.3 mAh g^{-1} and 67.8% to 99.6 mAh g^{-1} and 95.1% respectively; because of doping of Sn^{4+} in surface layer and moderate coating of SnO$_2$ on the surface occurring in the preparation processes. Based on the improvements as discussed above, it can be speculated that the dissolution of LiMn$_2$O$_4$ electrode into the electrolyte (as Mn^{2+}) decreases during the initial cycle owing to the doping of SnO$_2$ particles into the pristine LiMn$_2$O$_4$. And the capacity maintenance ability of composite cathode has been enhanced as a result of the SnO$_2$ coatings on the surface of LiMn$_2$O$_4$. Obviously, it does not mean that more content of favorable dopant will achieve better electrochemical performance. If the content of dopant is too much, unexpected impurities and deterioration of electrochemical performances will be ensued. In other words, there is usually a trade-off between cycle life and capacity in the case of the favorable dopant. In this work, the composite with 2% SnO$_2$ used as additive showed the best electrochemical performance.

4. CONCLUSION

The spherical SnO$_2$-modified LiMn$_2$O$_4$ is prepared based on controlled crystallization and solid state reaction in this study. SEM and XRD analysis show that the morphology and diffraction spectra of LiMn$_2$O$_4$ does not change obviously with the addition of SnO$_2$, revealing that the modification by SnO$_2$ does not destroy the crystal structure of pristine LiMn$_2$O$_4$. Some obvious impurities are observed in the samples with large content (wt. %) of SnO$_2$, indicating that some SnO$_2$ particles are coated on the surface of LiMn$_2$O$_4$ particles though some other SnO$_2$ have been introduced into the spinel structure. The ICP-AES results show that some Sn^{4+} ions have been doped into the surface layer of LiMn$_2$O$_4$ in place of Mn^{4+}.

There are no obvious differences observed in CV results between the first cycle and the tenth cycle, reflecting that the addition of SnO$_2$ does not destroy the electrochemical stability of LiMn$_2$O$_4$. EIS analysis shows that both R_{sf} (the resistance of solid electrolyte interface (SEI)) and R_{in} (the resistance between SEI film and cathode) are decreased and well stabilized as a result of the modification by SnO$_2$. Furthermore, the charge transfer resistance (R_{ct}) decreases with the increase of charge degree (SOC). In both cases, the SnO$_2$ coating and Sn^{4+} doping have a definite influence on the electrochemical performance, resulting in the decrease of impedance. Among all the samples, Sn (2%)/LMO composite display the smallest impedance.

The cycling performance shows that the addition of SnO$_2$ improves the ionic conductivity and the cycleability (the capacity and the capacity retention increase from 76.3 mAh g^{-1} and 67.8% to 99.6 mAh g^{-1} and 95.1%, respectively.) due to better crystal structural stability by the surface layer doping

of Sn^{4+}. The Sn (2%)/LMO composite displays the best electrochemical performance at different temperature and the best cycling performance at 55°C because of the moderate coating of SnO_2.

References

1. Y. Gao, J.R. Dahn. *J. Electrochem. Soc.* 143 (1996) 100.
2. A. Ogata, T. Shimizu, S. Komaba. *J. Power Sources* 174 (2007) 756.
3. X.M He, L. Wang W.H. Pu, G.Y. Zhang, C.Y. Jiang, C.R. Wan, *Int. J. Electrochem. Sci.* 1(2006)12.
4. X.M. He, J.J. Li, Y. Cai, Y.W. Wang, J.R. Ying, C.Y. Jiang, C.R. Wan, *J. Solid State Electrochem.* 9(2005)438.
5. Y. Cai,Y.W. Wang, X.M. He, C.Y. Jiang, C.R. Wan, *J. Inorg. Mat.* 19(2004)1058.
6. X.M. He, J.J. Li, Y. Cai, C.Y. Jiang, C.R. Wan, *Mat. Chem. Phys.* 95(2006)105.
7. X.M. He, J.J. Li, Y. Cai, Y.W. Wang, J.R. Ying, C.Y. Jiang, C.R. Wan, *Solid State Ionics*, 176(2005) 2571.
8. T. Aoshima, K. Okahara, C. Kiyohara, K. Shizuka. *J. Power Sources* 97-98 (2001) 377.
9. S. W. Lee, K. S. Kim, H. S. Moon, H. J. Kim, B. W. Cho, W. I. Cho, J. B. Ju, J. W. Park. *J. Power Sources* 126 (2004)150.
10. Y. K. Sun, K.J. Hong, J. Prakash. J. Electrochem. Soc.150 (2003) A970.
11. S. C. Park, Y. M. Kim, Y. M. Kang, K. T. Kim, P. S. Lee, J. Y. Lee. *J. Power Sources* 103 (2001) 86.
12. Y. K. Sun, K. J. Hong, J. Prakash, K. Amine. *Electrochemistry Communications* 4 (2002) 344.
13. L. J. Fu, H. Liu, C. Li, Y. P. Wu, E. Rahm, R. Holze, H. Q. Wu. *Prog. Mater. Sci.* 50 (2005) 881.
14. X. M. He, J. J. Li, Y. Cai, Y. W. Wang, J. R. Ying, C. Y. Jiang, C. R. Wan. *J. Power Sources* 150 (2005) 216.
15. X. Wu, S. B. Kim. J. Power Sources 109 (2002) 53.
16. D. Aurbach, M. D. Levi, E. Levi, H. Teller, B. Markovsky, G. Salitra, U. Heider, L. Heider. *J. Electrochem. Soc.* 145 (1998) 3024.
17. F. Nobili, S. Dsoke, F. Croce, R. Marassi. *Electrochim. Acta* 50 (2005) 2307.
18. Y. P. Wu, E. Rahm, R. Holze. *Electrochim. Acta* 47 (2002) 3491.
19. C. S. Wang, A. J. Appleby, F. E. Little. *Electrochim. Acta* 46 (2001) 1793.
20. A. Funabiki, M. Inaba, Z. Ogumi. *J. Power Sources* 68 (1997) 227.
21. K. N. Jung, S. I. Pyun, J. W. Lee. *Electrochim. Acta* 49 (2004) 4371.
22. H. Li, X. J. Huang, L.Q. Chen. *J. Power Sources* 81-82 (1999) 340.
23. C. L. Li, Z. W. Fu. *J. Electrochem. Soc.* 154 (2007) A784.
24. S. Q. Liu, S. C. Li, K. L. Huang, B. L. Gong, G. Zhang. *J. Alloys and Compounds*, *In Press.*
25. Y. C. Chang, H. J. Sohn. *J. Electrochem. Soc.* 147 (2000) 50.
26. M. Itagaki, N. Kobari, S. Yotsuda, K. Watanabe, S. Kinoshita, M. Ue. *J. Power Sources* 135 (2004) 255.
27. Z. H. Yang, S. B. Sang, Y. Feng, Y. H. Zhou, K. L. Huang, H. Q. Wu. *Diamond Relat. Mat.* 14 (2005) 1302.
28. S. Zhang, P. F. Shi. Electrochim. Acta 49 (2004) 1475.
29. T. H. Piao, S. M. Park, C. H. Doh, S. I. Moon. *J. Electrochem. Soc.* 146 (1999) 2794.

30. K. N. Jung, S. I. Pyun. *Electrochim. Acta* 52 (2007) 5453.
31. M. Quintin, O. Devos, M. H. Delville, G. Campet. *Electrochim. Acta* 51 (2006) 6426.
32. M. G. S. R. Thomas, P. G. Bruce, J. B. Goodenough. *J. Electrochem. Soc.* 132 (1985) 1521.
33. J. E. Bauerle. *J. Phys. Chem. Solids* 30 (1969) 2657.
34. P. R. Sorensen, T. Jacobsen. *Electrochim. Acta* 27 (1982) 1671.
35. C. A. C. Sequeira, A. Hooper. *Solid State Ionics* 9-10 (1983) 1131.
36. D. Fauteux. *Solid State Ionics* 17 (1985) 133.
37. J. G. Li, X. M. He, R. S. Zhao, C. R. Wan, C. Y. Jiang, D. G. Xia, S. C. Zhang. *J. Power Sources* 158 (2005) 524.
38. G. G. Amatucci, N. Pereira, T. Zheng, J.M. Tarascon. *J. Electrochem. Soc.* 148 (2001) A171.
39. B. Deng, H. Nakamura, M. Yoshio. *Chem. Lett.* 32 (2003) 942.
40. T. Horiba, K. Hironaka, T. Matsumura, T. Kai, M. Koseki, Y. Muranaka. *J. Power Sources* 119-121 (2003) 893.
41. S.H. Guo, S.C. Zhang, X. M. He, W.H. Pu, C.Y. Jiang, C.R. Wan. *J. Electrochem. Soc.* 155 (2008) A760.
42. J.S. Zhao, L. Wang, X.M. He, C.R. Wan, C.Y. Jiang, *Int. J. Electrochem. Sci.* 5(2010) 478.